ORIGINAL PAPER

Post-injection spreading and trapping of CO_2 in saline aquifers: impact of the plume shape at the end of injection

Christopher W. MacMinn · Ruben Juanes

Abstract We use an analytical model for the post-injection spreading of a plume of CO_2 in a saline aquifer under the action of buoyancy and capillary trapping to show that the spreading behavior is at all times strongly influenced by the shape of the plume at the end of the injection period. We solve the spreading equation numerically and confirm that, at late times, the volume of mobile CO_2 is given by existing asymptotic analytical solutions. The key parameters governing plume spreading are the mobility ratio, M, and the capillary trapping number, Γ—the former sets the shape of the plume at the end of the injection period, and the latter sets the amount of trapping. As a quantitative measure of the dependence of the spreading behavior on the initial shape, we use a volume ratio. That is, we evolve the plume from a true end-of-injection initial shape and also from an idealized "step" initial shape, and we take the ratio of these mobile plume volumes in the asymptotic regime. We find that this volume ratio is a power-law in M, where the exponent is governed exclusively by Γ. For conditions that are representative of geologic CO_2 sequestration, the ratio of mobile volumes between "true" and "step" initial plume shapes can be 50% or higher.

1 Introduction

Storage of carbon dioxide in geological formations is widely regarded as a promising tool for reducing global atmospheric CO_2 emissions (see, e.g., [1–5]). To evaluate reservoir fill and assess leakage risks, an accurate understanding of the subsurface spreading and migration of the plume of mobile CO_2 during and after injection, including its shape, size, and extent, is essential.

1.1 Saline aquifers and trapping mechanisms

Among the geological formations well-suited for use as storage sites are deep saline aquifers (see, e.g., [1, 4, 5]). The properties of the CO_2 vary with the temperature and pressure at depth—typically, CO_2 is less dense and much less viscous than the resident groundwater, and will migrate upward due to buoyancy and spread along the top boundary of the aquifer during and after injection. When upward migration of mobile CO_2 is blocked by an impermeable layer, it is said to be *structurally* trapped [5]. Structural trapping is effective but unreliable, as the CO_2 remains mobile—a pre-existing well or the activation of a fault could lead to leakage into shallower formations.

However, it is well-known that some amount of CO_2 will be trapped in the pore space of the aquifer rock at the trailing edge of the plume as it migrates and spreads [5–8]. This phenomenon, known as capillary trapping, occurs in flow through a porous medium as a

C. W. MacMinn · R. Juanes (✉)
Massachusetts Institute of Technology,
77 Massachusetts Avenue, Bldg. 48,
Cambridge, MA 02139, USA
e-mail: juanes@mit.edu

C. W. MacMinn
e-mail: cmac@mit.edu

non-wetting fluid (here, CO_2) is displaced by a wetting one (here, groundwater) from the pore space of the rock (i.e., during imbibition). Capillary trapping is an ideal mechanism for the geological storage of CO_2 because the trapped gas is immobile and distributed over a large area, greatly decreasing the risk of leakage and enhancing the effectiveness of chemical trapping mechanisms such as dissolution and mineral deposition, which act on a much longer timescale [6, 7]. The fraction of pore space occupied by trapped or *residual* CO_2 after the bulk is displaced is known as the residual gas saturation, S_{gr}; similarly, some fraction of pore space may be occupied by immobile groundwater, and this fraction is known as the connate water saturation, S_{wc}.

1.2 Previous work

The injection of mobile, buoyant CO_2 into a saline aquifer and its subsequent migration falls into the broad class of fluid-mechanics problems known as viscous gravity currents, wherein a finite amount or flux of one fluid is released into a second, ambient fluid. The introduced fluid having a different density from the ambient fluid, the flow is governed by the balance of buoyancy and viscous dissipation.

Several cases of a fluid being released or injected into a less dense ambient fluid on a flat surface were considered by Huppert [9] for both planar and axisymmetric geometries; see references therein for earlier work on gravity currents. Barenblatt [10] considered a similar problem, the slumping of an axisymmetric "mound" of groundwater in a porous medium filled with a less-dense, less-viscous ambient fluid. Flow in a porous medium introduces several additional complications over unconstrained flow—of primary interest here is capillary trapping, which causes the volume of the mound to decrease as it slumps. Capillary trapping is not included in [10], but Kochina et al. [11] solve the same problem including capillary trapping; Barenblatt [12] describes both solutions.

In geological CO_2 storage in a saline aquifer, the introduced fluid—CO_2—is *less* dense and much less viscous than the ambient fluid—brine—and it spreads along the top boundary of the domain rather than slumping along the bottom boundary. Similar systems have been considered by Dussan and Auzerais [13] and by Huppert and Woods [14], although neither considers capillary trapping.

On the specific topic of the geological storage of CO_2 in a saline aquifer, much work has been done quite recently. Numerical studies include [6–8, 15], among many others. Here, however, we are interested in the effect of the shape of the plume at the end of the injection period on the plume evolution over long periods of time, in the period when the plume becomes very thin and widespread—this type of study is difficult with a typical numerical simulator, but is a particular strength of theoretical models, so these will be our focus here.

Nordbotten et al. [16] develop a model for the shape of the CO_2 plume during radially outward injection, giving an analytical solution for the case when advective viscous effects dominate diffusive buoyancy effects, which is often the case during the injection period; they demonstrate favorable comparison of their results with numerical simulations. Nordbotten and Celia [17] show a different development of the model for the injection period, giving again the analytical solution for advection-dominated flow; they then include some dissolution effects with very good agreement between analytical and numerical results. The flow of CO_2 during injection is purely outward when buoyancy is neglected, so capillary trapping does not play a role in their studies.

Hesse et al. [18] consider the post-injection spreading and migration of a planar plume of CO_2, developing a model for the plume shape both without and with capillary trapping that also includes a sloping caprock, along which the plume will migrate; they develop scaling laws for the plume volume, maximum thickness, and overall extent for a horizontal aquifer that agree well with numerical solutions, and comment on the sloping-aquifer case. Hesse et al. [19] give early- and late-time similarity solutions for spreading in a horizontal aquifer without trapping. Hesse et al. [20] introduce capillary trapping to this problem, showing that the early-time spreading is self-similar in the planar geometry; they also comment on and give scalings for the late-time spreading behavior, and further develop a solution for the case when the aquifer is not horizontal and up-slope migration dominates buoyant spreading.

In geological CO_2 storage, the initial condition for post-injection spreading and migration is the shape of the plume at the end of the injection period. The post-injection upward spreading of the plume against the caprock has a diffusive mathematical character in all of the models discussed above, and it is well-known that diffusive models typically "lose information" about initial conditions over time [12]; it is then commonly argued that the initial shape of the plume for post-injection spreading is unimportant because the time scales of interest are long and the spreading behavior eventually becomes independent of the details of the initial shape. This is the case when capillary trapping is not considered, but the inclusion of capillary trapping causes the plume evolution to depend for all time on the details of the initial shape [11, 12]; Hesse et al.

make note of this, but they in all cases take the end-of-injection plume shape to be a "step."

Juanes and MacMinn [21, 22] model the planar post-injection migration of a CO_2 plume for the case where advection due to net natural groundwater flow through the aquifer dominates diffusive spreading due to buoyancy, including the effect of capillary trapping and accounting for the true shape of the plume at the end of injection. Their results demonstrate that the end-of-injection shape plays a strong role in determining the overall plume footprint.

Here, we study the post-injection spreading of an axisymmetric plume of CO_2 in a horizontal aquifer under the action of buoyancy and capillary trapping, with no groundwater through-flow, and we show that the particular end-of-injection plume shape has a strong influence on the spreading behavior at all times.

2 Theoretical model for CO_2 spreading

We briefly outline the derivation of the spreading equation, following [18, 20]. We take the aquifer to be homogeneous, isotropic, and horizontal, and with no net groundwater through-flow. We take the fluids to be incompressible and Newtonian, with constant and uniform properties—this does not require that variation in fluid properties with temperature and pressure be completely neglected, but rather that variations of these properties *within the aquifer* are neglected.

We employ a sharp-interface approximation, neglecting the width of typical gradients in saturation (i.e., the capillary transition zone or "fringe") compared to typical length scales in the horizontal and vertical directions, and we further neglect the capillary pressure compared to typical hydrostatic and viscous pressure drops; see, e.g., [23, 24].

We make the Dupuit or "vertical equilibrium" approximation and neglect the vertical flow velocity compared to the horizontal flow velocity. This approximation is justified when the characteristic vertical length scale is much smaller than the characteristic horizontal one, $H/R_c \ll 1$. This is generally the case for aquifers, which are typically very thin compared to their horizontal dimensions; see again, [23, 24].

In accordance with the sharp-interface approximation, we divide the domain into three regions, each of uniform CO_2 and groundwater saturation and with discontinuous saturations across region–region boundaries. As illustrated in Fig. 1, region 1 contains mobile CO_2 with a saturation S_{wc} of connate groundwater, region 2 contains mobile groundwater with a saturation S_{gr} of trapped CO_2, and region 3 contains mobile
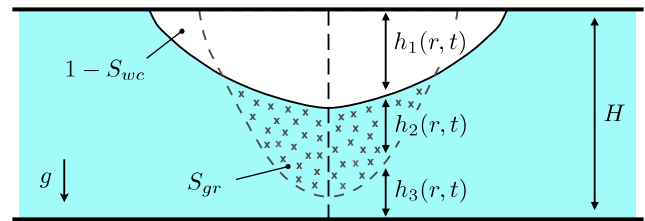

Fig. 1 The domain is divided into three regions of uniform CO_2 and groundwater saturation separated by sharp interfaces corresponding to saturation discontinuities. Region 1 (*white*) has a saturation $1 - S_{wc}$ of mobile CO_2 with a saturation S_{wc} of connate groundwater; region 2 (*blue with gray exes*) has a saturation S_{gr} of trapped CO_2 and a saturation $1 - S_{gr}$ of mobile groundwater; region 3 (*blue*) contains only mobile groundwater. The plume is axially symmetric, where the *vertical dashed black line* indicates the axis of symmetry and coincides with the injection well. The profile of the plume at an earlier time is also shown, outlined in *dashed gray*

groundwater with no CO_2. The aquifer has a total thickness H, and the thickness of region i, $i = 1, 2, 3$, at a radial position r and time t is denoted $h_i(r, t)$, where r is measured from the axis of symmetry of the plume. Gravity acts downward.

Under these assumptions, we can write the Darcy velocity for each phase in each region and relate them through conservation of mass, accounting carefully for the residual fluid that crosses each interface [18, 20]. We write the resulting spreading equation,

$$\tilde{R} \frac{\partial h_1}{\partial t} - \kappa \frac{1}{r} \frac{\partial}{\partial r} \left(r[1 - f(h_1, h_2, h_3)]h_1 \frac{\partial h_1}{\partial r} \right) = 0, \quad (1a)$$

$$\tilde{R} = \begin{cases} 1 & \text{if } \partial h_1/\partial t > 0, \\ 1 - \Gamma & \text{if } \partial h_1/\partial t < 0, \end{cases} \quad (1b)$$

$$\kappa = \frac{\Delta \rho g k \lambda_1}{\phi(1 - S_{wc})}, \quad (1c)$$

$$f(h_1, h_2, h_3) = \frac{\lambda_1 h_1}{\lambda_1 h_1 + \lambda_2 h_2 + \lambda_3 h_3}, \quad (1d)$$

$$\frac{\partial h_1}{\partial t} = \begin{cases} -\dfrac{\partial h_3}{\partial t} & \text{if } \partial h_1/\partial t > 0 \text{ and } h_2 = 0, \\ -\dfrac{\partial h_2}{\partial t} & \text{otherwise,} \end{cases} \quad (1e)$$

where $\Delta \rho = \rho_w - \rho_g$ is the density difference between the groundwater and the CO_2, g is the force per unit mass due to gravity, and k and ϕ are the intrinsic permeability and porosity of the aquifer, respectively. The discontinuous accumulation coefficient $\tilde{R}$ takes different values for drainage (h_1 increasing) and imbibition (h_1 decreasing), capturing the loss of volume due to capillary trapping—the relationship Eq. 1e similarly reflects the difference between imbibition, when CO_2

is trapped, and drainage, when it is not. The parameter $\Gamma = S_{gr}/(1 - S_{wc})$ is the capillary trapping number, which measures the fraction of CO_2 that is left behind at the imbibition front and takes a constant value between zero (no trapping) and one. $\lambda_i = k_{ri}/\mu_i$ is the mobility of the mobile phase in region i, $i = 1, 2, 3$, where k_{ri} and μ_i are the relative permeability to that phase and the viscosity of that phase, respectively.

We expect the relative permeability to groundwater in region 2 to be less than that in region 3 because of the presence of the trapped gas there. In order to make analytical progress, however, we explicitly neglect this effect and assume that $\lambda_2 = \lambda_3$. This simplifies Eq. 1 substantially because the distinction between regions 2 and 3 no longer has physical significance, and the nonlinear function $f(h_1, h_2, h_3)$ can be rewritten as a function of h_1 only,

$$f(h_1) = \frac{\lambda_1 h_1}{\lambda_1 h_1 + \lambda_3 (H - h_1)}. \tag{2}$$

With Eq. 2, Eq. 1 agrees with the spreading equation of [18, 20], but here for an axisymmetric plume. We write Eq. 1 in dimensionless form,

$$\tilde{R} \frac{\partial \eta}{\partial \tau} - \frac{1}{\xi} \frac{\partial}{\partial \xi} \left(\xi [1 - f(\eta)] \eta \frac{\partial \eta}{\partial \xi} \right) = 0, \tag{3a}$$

$$\tilde{R} = \begin{cases} 1 & \text{if} \quad \partial \eta/\partial \tau > 0, \\ 1 - \Gamma & \text{if} \quad \partial \eta/\partial \tau < 0, \end{cases} \tag{3b}$$

$$f(\eta) = \frac{M\eta}{M\eta + (1 - \eta)}, \tag{3c}$$

where $\eta = h_1/H$, $\tau = t/T_c$, $\xi = r/R_c$, and $M = \lambda_1/\lambda_3$ is the mobility ratio. We choose the characteristic time T_c to be equal to the diffusive timescale $T_c = R_c^2/(H\kappa)$, and we choose the characteristic length scale R_c to be the radius R_0 of a cylinder of volume $V_0/\phi(1 - S_{wc})$ and height H, where V_0 is the volume of the plume at the end of injection, $R_c = R_0 = \sqrt{V_0/(\pi H \phi (1 - S_{wc}))}$. Equation 3 takes only two parameters, M and Γ. The parameter κ does not appear explicitly—it influences only the characteristic timescale. We seek continuous solutions $\eta(\xi, \tau)$ to Eq. 3 with continuous flux $[1 - f(\eta)]\eta\eta_\xi$, for some axially symmetric initial shape $\eta(\xi, \tau = 0) = \eta_0(\xi)$.

2.1 The shape of the plume at the end of injection

The shape of the plume at the end of the injection period serves as the initial condition for the post-injection spreading problem. Nordbotten et al. [17] provide an explicit analytical solution for the plume shape during the injection period, valid when gravity is negligible relative to the flow induced by injection. By comparing this negligible-gravity solution to a numerical solution for the full injection model, Nordbotten et al. find that this assumption is valid when

$$\frac{2\pi \Delta\rho g k \lambda_1 H}{Q_i/H} \ll M, \tag{4}$$

where Q_i is the volumetric rate of injection.

The end-of-injection plume shape from this solution, which we denote η_0, is given by

$$\eta_0(\xi) = \begin{cases} 1 & \text{if} \quad 0 \le \xi \le 1/\sqrt{M}, \\[2mm] \left(\frac{1}{M-1} \right) \left(\frac{\sqrt{M}}{\xi} - 1 \right) & \text{if} \quad 1/\sqrt{M} < \xi < \sqrt{M}, \\[2mm] 0 & \text{if} \quad \xi \ge \sqrt{M}, \end{cases} \tag{5}$$

for $M > 1$. For $M = 1$, the solution degenerates to a "step" or cylinder:

$$\eta_0(\xi) = \begin{cases} 1 & \text{if} \quad 0 \le \xi \le 1, \\[2mm] 0 & \text{if} \quad \xi \ge 1. \end{cases} \tag{6}$$

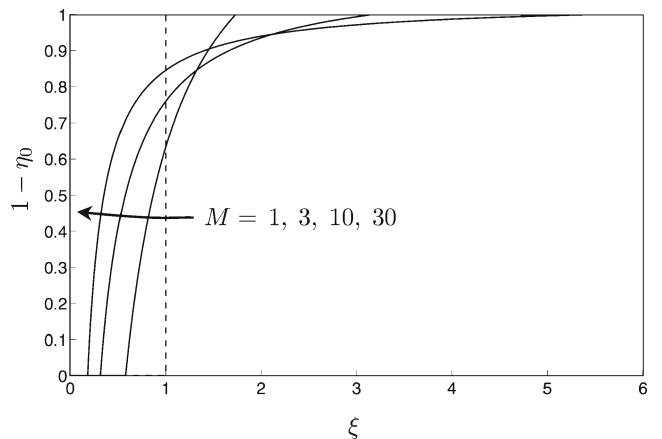We plot these end-of-injection plume shapes in Fig. 2.

Fig. 2 The shape of the CO_2 plume at the end of injection is plotted here for several mobility ratios—the plume shape is calculated from Eq. 6 for $M = 1$ (*dashed line*), and from Eq. 5 for $M = 3$, 10, and 30 (*solid lines*). The plume is axisymmetric about $\xi = 0$, which corresponds to the injection well. The plume volume is the same in all cases—note that the so-called "tonguing" of the profile increases dramatically as M increases

3 Asymptotic analytical solutions to the spreading equation

Barenblatt [12] describes the solution to a slumping problem, wherein the slumping fluid is water and the ambient fluid is a gas—in this case, the density and viscosity of the ambient fluid are neglected, and the governing equation is of the form

$$\tilde{R}\frac{\partial h_1}{\partial t} - \kappa\frac{1}{r}\frac{\partial}{\partial r}\left(rh_1\frac{\partial h_1}{\partial r}\right) = 0, \tag{7}$$

where the coefficient $\tilde{R}$ is conditional as in Eq. 1. The two equations agree exactly in the limit $f \ll 1$, corresponding to $h_1 \ll H/M$. This is a reasonable assumption from the outset in Barenblatt's slumping problem, where the mobility of the slumping fluid is taken to be much smaller than the mobility of the ambient fluid, $M \ll 1$, and where the domain is taken to be unbounded in the vertical direction, $h_1 \ll H$. This is generally not justified in geological CO_2 storage, where the mobility of the CO_2 is typically much larger than that of the ambient groundwater, $M \gg 1$, and the plume initially fills the entire thickness of the aquifer; however, the spreading problem does eventually reach the same limit as the plume becomes very thin, which can be considered a "late-time" regime.

Equation 3 does not have a known analytical solution, and must be solved numerically. As the plume becomes very thin, however, we expect the numerical solutions to Eq. 3 to converge asymptotically to the analytical solutions to Eq. 7. Next, we recall the analytical solutions to Eq. 7 provided by [11, 12]. These help us validate the numerical solutions and provide physical insight into the late-time plume evolution.

3.1 Asymptotic solution for spreading without trapping

When capillary trapping is not considered, the coefficient $\tilde{R}$ in Eq. 7 takes the constant value 1 and [12] shows that the equation is satisfied by a similarity solution.

First, we observe that the plume thickness h_1 may be a function of time, space, the parameter κ, the aquifer thickness, and the end-of-injection shape of the plume, which can be fully characterized by M and two of the three parameters H, R_0, and V_0. We therefore write

$$h_1 = h_1(r, t, M, \hat{V}_0, R_0), \tag{8}$$

where $\hat{V}_0 = V_0/\phi(1 - S_{wc})$ is the volume of porous medium filled by the initial fluid volume V_0. Dimen-

sional analysis then reveals that the problem can be expressed in terms of the four dimensionless groups,

$$\Pi_1 = h_1\left(\frac{\kappa t}{\hat{V}_0}\right)^{1/2}, \quad \Pi_2 = r\left(\frac{1}{\hat{V}_0\kappa t}\right)^{1/4},$$

$$\Pi_3 = R_0\left(\frac{1}{\hat{V}_0\kappa t}\right)^{1/4}, \quad \Pi_4 = M, \tag{9}$$

such that the solution takes the form $\Pi_1 = F(\Pi_2, \Pi_3)$ with parameter Π_4. Since Π_3 shrinks as time increases, the asymptotic solution can be expressed as $\Pi_1 = F(\Pi_2)$ in the limit $\Pi_3 \to 0$. Because the details of the end-of-injection plume shape are contained in Π_3 and Π_4, the solution is valid asymptotically for an arbitrary end-of-injection shape. Proceeding with the mechanics of the similarity solution, the result is

$$\Pi_1 = F(\Pi_2) = F_0 - \frac{1}{8}\Pi_2^2, \tag{10}$$

where the constant F_0 is determined by requiring that the volume of the plume be conserved, a condition that can be applied analytically in this case. The result [12] in dimensionless form is

$$\eta(\xi, \tau) = \left(\frac{1}{\tau}\right)^{1/2}\left[\frac{1}{2} - \frac{1}{8}\xi^2\left(\frac{1}{\tau}\right)^{1/2}\right], \tag{11}$$

valid for $\xi, \eta \geq 0$. This solution is entirely independent of the initial plume shape.

Equation 11 is a solution to Eq. 7, valid asymptotically for an arbitrary initial plume shape of volume V_0 in the limit as $\Pi_3 \to 0$, i.e., for $(\pi\tau)^{1/4} \gg 1$. Similarly, we expect Eq. 11 to be a solution to Eq. 3, valid asymptotically for $\Pi_3 \to 0$ and $f \ll 1$, i.e., for $(\pi\tau)^{1/4} \gg 1$ and $\eta \ll 1/M$, respectively. We use the maximum plume thickness (the thickness at the axis) from Eq. 11 to estimate the time at which the latter criterion is satisfied, and we find that $\eta \ll 1/M$ when $2\tau^{1/2} \gg M$; this estimate serves as a lower bound on the range of validity of Eq. 11 as a solution to Eq. 3 without trapping, because f slows the plume evolution while it is non-negligible compared to 1. In general, we can then expect solutions for larger values of M to take longer to converge to this asymptotic behavior.

3.2 Asymptotic solution for spreading with trapping

When capillary trapping is included, the coefficient $\tilde{R}$ becomes discontinuous and the method from Section 3.1 can no longer produce a smooth solution. Barenblatt [12] shows that this is because the assumption that the plume evolution becomes independent of Π_3 as $\Pi_3 \to 0$ is no longer valid, i.e., the plume evolution never becomes independent of the initial shape.

Equation 7 is instead satisfied by a similarity solution *of the second kind*.

The capillary trapping number, which now enters the problem through $\tilde{R}$, forms a fifth dimensionless group, $\Pi_5 = \Gamma$. The fact that a physical solution of the form $\Pi_1 = F(\Pi_2)$ does not exist as $\Pi_3 \to 0$ implies that the solution does not become independent of Π_3 in this limit, and the solution is assumed to be of the form

$$\frac{\Pi_1}{\Pi_3^{\gamma}} = F_1\left(\zeta = \frac{\Pi_2}{\Pi_3^{\delta}}\right), \qquad (12)$$

where the exponents γ and δ cannot be determined through dimensional analysis alone, and must instead be determined in the course of the solution—a hallmark of such similarity solutions of the second kind. The result [11, 12] in dimensionless form is

$$\eta(\xi, \tau) = \left(\frac{\hat{B}^2}{\tau^{1-2\beta}}\right) F_1\left(\zeta = \frac{\xi}{\hat{B}\tau^{\beta}}\right), \qquad (13)$$

where the constant $\hat{B}$ remains unknown and the function $F_1(\zeta)$ results from the numerical solution of a system of second-order ordinary differential equations. The constant β is an eigenvalue of the solution—for any given value of Γ, there exists only one particular value of β for which the function $F_1(\zeta)$ can satisfy the appropriate boundary conditions. We plot β against Γ in Fig. 3. See [11, 12, 25] for a more detailed description.

As in the no-trapping case, the final constant in Eq. 13, $\hat{B}$, is set by a condition on the volume of the plume. The analytical solution is an asymptotic description of the plume evolution, and there is some "early"

period during which the asymptotic solution clearly does not apply. Because of this, we must in some way match the asymptotic solution with the general solution as the general solution converges to this asymptotic behavior. Without capillary trapping, we simply require that the volume of the plume in the asymptotic regime be equal to the initial volume of the plume. With capillary trapping, the volume of the plume is no longer conserved; it will instead decrease by some unknown amount as CO_2 is trapped in the plume's wake during the transitional period. To determine how much plume volume is lost during the transitional period and fix the value of the constant $\hat{B}$, then, we solve Eq. 3 numerically until the plume evolution enters the asymptotic regime, and then match the volume of the plume from the analytical solution with the volume of the plume from the numerical solution at some arbitrary time in the asymptotic regime. The details of the initial plume shape then enter the asymptotic solution through $\hat{B}$.

Integrating Eq. 13 over the domain gives a power-law scaling in time for the volume of the plume,

$$\hat{V} = C \tau^{4\beta-1}, \qquad (14)$$

where C is a constant that depends on $\hat{B}$ and $F_1(\zeta)$ and, therefore, on the initial plume shape and the amount of capillary trapping. Because it is only the constant C that depends on the initial plume shape, the plume evolution for any initial shape will converge to a power-law with exponent $4\beta - 1$ that is smaller (more negative) for larger Γ, i.e., the plume volume will shrink faster for larger Γ. However, the actual value of the plume volume at any time in the asymptotic regime will
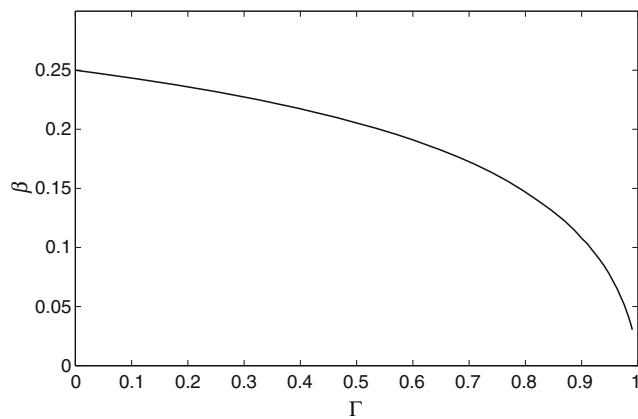

Fig. 3 The eigenvalue β in Eq. 13 plotted against the capillary trapping number Γ. For each value of Γ, there is a single value of β for which a solution $F_1(\zeta)$ exists. Note that $\beta \to 1/4$ as $\Gamma \to 0$, at which point Equations 13 and 11 have the same form—i.e., the asymptotic solution with capillary trapping converges smoothly to the solution without trapping as the amount of trapping goes to zero
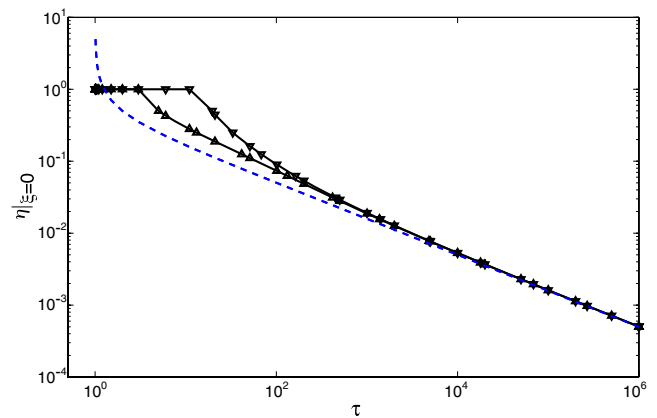

Fig. 4 Time-evolution of the thickness of the CO_2 plume at its axis of symmetry ($\xi = 0$) without capillary trapping ($\Gamma = 0$) for $M = 20$. Numerical solutions to Eq. 3 (*solid black lines*) are shown starting from the "true" initial shape for $M = 20$ (*upward-pointing triangle markers*) and the "step" initial shape (*downward-pointing triangle markers*); the asymptotic analytical solution from Eq. 11 is also shown (*dashed blue line*)
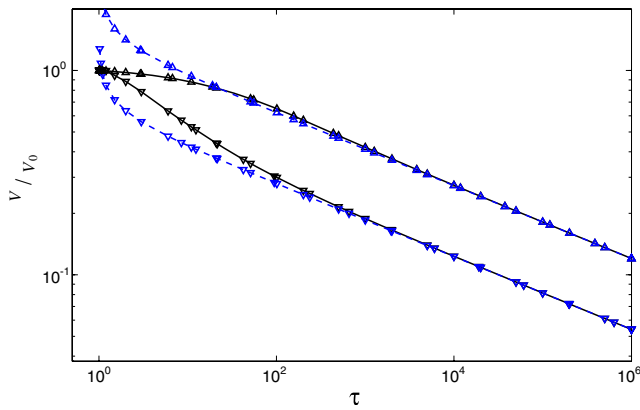
Fig. 5 Time-evolution of the volume of the CO_2 plume with capillary trapping, for $\Gamma = 0.5$ and $M = 20$. Numerical solutions to Eq. 3 (*solid black lines*) and asymptotic analytical solutions from Eq. 13 (*dashed blue lines*) are shown starting from the "true" initial shape for $M = 20$ (*upward-pointing triangle markers*) and the "step" initial shape (*downward-pointing triangle markers*). Volume is normalized by the initial volume. The solutions for the two different initial shapes no longer converge to the same asymptotic power-law—the rate of decay is the same in both cases, but there is a gap between the curves because substantially different amounts of CO_2 are trapped as the plume transitions from the different initial shapes to the asymptotic behavior

depend strongly on the value of C, and therefore on the details of the initial shape.

4 Impact of the initial plume shape

To study the effect of the initial plume shape on the long-term plume evolution, we solve Eq. 3 numerically using a finite-volume method. In the limit, as the plume becomes thin, these numerical solutions converge to the asymptotic analytical behavior described in Section 3.

We evolve the plume from two different initial shapes for several values of M, and for several values of Γ at each M. For the two initial shapes, we use the end-of-injection shape from Eq. 5 for the appropriate value of M, and also the end-of-injection shape from Eq. 6, the latter being equivalent to taking $M = 1$ during injection—we refer to these in what follows as the "true" and "step" initial shapes, respectively.

Without capillary trapping (i.e., $\Gamma = 0$), we expect the solution for any arbitrary initial plume shape of volume V_0 to converge to the asymptotic solution as the plume becomes thin. We illustrate this in Fig. 4,
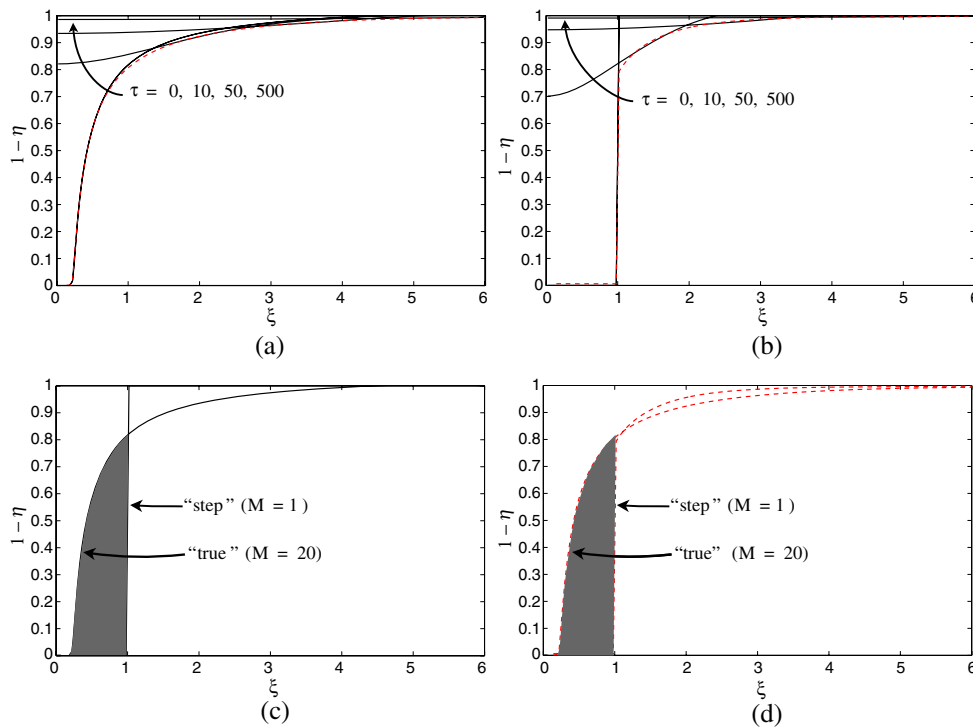

Fig. 6 The shape of the CO_2 plume (*solid black lines*) at several times during post-injection spreading for $M = 20$ and $\Gamma = 0.5$, starting from **a** a "true" initial shape and **b** a "step" initial shape; the envelopes of the region containing trapped gas at $\tau = 500$ are also shown (*dashed red lines*). These two initial shapes are plotted together in **c** with the volume between them *shaded in grey*—the plume will retreat from this area as it evolves from the

"step" initial profile, leaving trapped gas behind. The envelopes of the region containing trapped gas at $\tau = 500$ for the "true" and "step" initial shapes are shown in **d** (*dashed red lines*) overlaid on the grey region from **c**. It is clear from **c** and **d** that the difference in initial shapes translates directly to substantially different amounts of trapping as the plume evolves

in which we plot the time evolution of the thickness of the CO_2 plume at its axis for $M = 20$ for both the "true" and "step" initial shapes. Figure 4 shows that the plume evolution converges to the same asymptotic solution for both initial shapes as the plume becomes thin. Behavior for other values of M is qualitatively similar, but both the gap that initially exists between the two numerical solutions and the time it takes for the numerical solutions to converge to the asymptotic solution increase with M. The reason for the former is that the "true" and "step" initial plume shapes are increasingly different as M increases, as illustrated in Fig. 2; the reason for the latter is that it takes longer to reach the limit $\eta \ll 1/M$ for larger M. Figure 4 also serves as a qualitative demonstration that the numerical solution provides sufficiently accurate results over long periods of time.

With capillary trapping, the asymptotic behavior is not independent of the initial plume shape because the amount of CO_2 that is trapped depends on the details of the initial shape. In Fig. 5, we plot the time evolution of the volume of the CO_2 plume for $\Gamma = 0.5$ and $M = 20$ for the "true" and "step" initial shapes. The volume of the plume converges to an asymptotic power-law with the same rate of decay in both cases, but there is a gap between the curves because substantially different amounts of CO_2 are trapped during the transition from the initial shape toward the asymptotic behavior. Behavior for other values of Γ and M is qualitatively similar. As for the no-trapping case, the gap that initially exists between the two numerical solutions and the time it takes for the numerical solutions to converge to the asymptotic solution both increase with M. Unlike the no-trapping case, however, this initial gap between the two numerical solutions never closes—the two solutions are separated for all time.

The qualitative reason for this behavior is shown in Fig. 6, in which we plot the plume shape at several times for the "true" and "step" initial shapes, and we compare the envelopes of the region containing trapped CO_2 for the two cases. The difference in initial shapes translates directly to substantially different amounts of trapping as the plume evolves, even for relatively early times.

We have shown that evolving the plume from a "step" initial shape instead of the "true" initial shape *under*-predicts the plume volume at later times because it *over*-predicts the amount of trapping that occurs at earlier times. We now evaluate the magnitude of this effect. Because the rate of decay in the asymptotic regime depends only on Γ, the ratio of the volumes at any time in the asymptotic regime for any two initial shapes is constant—this is clear from Eq. 14. We therefore calculate the ratio of the volume of the plume, V_1,

at some time in the asymptotic regime for the "step" initial condition to the volume of the plume, V_M, at the same time for the "true" initial condition, and we plot this ratio against M for several values of Γ (Fig. 7). This ratio is equal to 1 for $M = 1$, i.e., when the "step" and "true" initial shapes are the same, and decreases with increasing M as the two initial shapes become increasingly different and the "step" initial shape under-predicts the plume volume at late times (over-predicts the trapping at early times) by an increasingly large amount. The volume ratio also decreases as Γ increases because this increases the amount of trapping at all times. In fact, the volume ratio V_1/V_M displays a perfect power-law behavior in M:

$$\frac{V_1}{V_M} = C M^{-s}, \tag{15}$$

where the exponent s is a function of the capillary trapping number. The "step" initial shape under-predicts the volume of the plume by a factor of two or more for even moderate M and Γ.
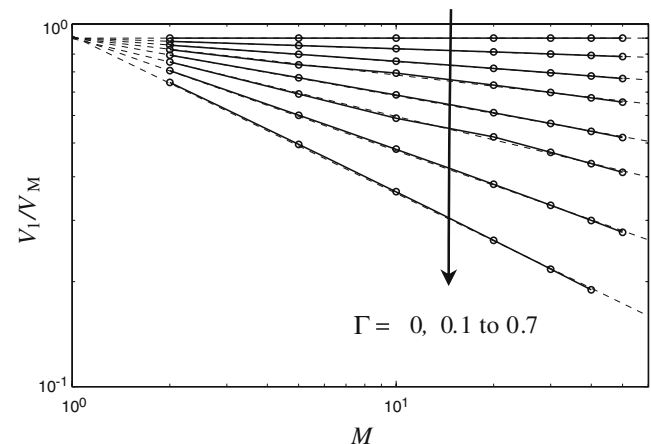

Fig. 7 The ratio of the volume of the plume having been evolved from a "step" initial shape (V_1) to the volume of the plume having been evolved from the "true" initial shape (V_M) at an arbitrary time in the asymptotic regime, plotted against M (*solid black lines with circle markers*) for $\Gamma = 0$ to 0.7 in increments of 0.1, as indicated. For given M and Γ, this volume ratio is constant in the asymptotic regime. The volume ratio is 1 for $\Gamma = 0$, and is a power-law in M with an exponent that decreases (becomes more negative) as Γ increases—a linear regression of $\log(V_1/V_M)$ against $\log(M)$ at each value of Γ is also shown (*dashed black lines*). Consider, for example, the case of $M = 20$ and $\Gamma = 0.5$—the volume ratio is approximately 0.45, meaning that evolution from the "step" initial shape under-predicts the plume volume at any time in the asymptotic regime by a factor of 0.45, or over-predicts the amount of CO_2 that has been trapped by more than a factor of 2

5 Conclusions

We have shown that the post-injection spreading of the CO_2 plume under the action of buoyancy and capillary trapping is strongly influenced by the shape of the plume at the end of the injection period. The key parameters in the asymptotic spreading behavior are the mobility ratio, M, and the capillary trapping number, Γ. The former sets the end-of-injection shape of the plume, and the latter sets the amount of trapping and, therefore, the strength of dependence on the end-of-injection plume shape, and also the rate of decay in the asymptotic power-law regime.

These results indicate that models for subsurface CO_2 spreading and migration should account for the true end-of-injection plume shape in order to predict the thickness, volume, or footprint of the mobile plume over time.

References

1. Bachu, S., Gunter, W.D., Perkins, E.H.: Aquifer disposal of CO_2: hydrodynamic and mineral trapping. Energy Convers. Manag. **35**(4), 269–279 (1994)
2. Lackner, K.S.: Climate change: a guide to CO_2 sequestration. Science **300**(5626), 1677–1678 (2003)
3. Schrag, D.P.: Preparing to capture carbon. Science **315**(5813), 812–813 (2007)
4. Orr, F.M.: Storage of carbon dioxide in geological formations. J. Pet. Technol. **56**(9), 90–97 (2004)
5. IPCC: Carbon dioxide capture and storage. Special report prepared by working group III of the intergovernmental panel on climate change. Intergovernmental Panel on Climate Change, Cambridge (2005)
6. Flett, M., Gurton, R., Taggart, I.: The function of gas-water relative permeability hysteresis in the sequestration of carbon dioxide in saline formations. In: SPE Asia Pacific Oil and Gas Conference and Exhibition, Perth, Australia, (88485-MS) (2004)
7. Juanes, R., Spiteri, E.J., Orr, F.M. Jr., Blunt, M.J.: Impact of relative permeability hysteresis on geological CO_2 storage. Water Resour. Res. **42**, W12418 (2006)
8. Kumar, A., Ozah, R., Noh, M., Pope, G.A., Bryant, S., Sepehrnoori, K., Lake, L.W.: Reservoir simulation of CO_2 storage in deep saline aquifers. SPE J. **10**(3), 336–348 (2005)
9. Huppert, H.E.: The propagation of two-dimensional and axisymmetric viscous gravity currents over a rigid horizontal surface. J. Fluid Mech. **121**, 43–58 (1982)
10. Barenblatt, G.I., Entov, V.M., Ryzhik, V.M.: Theory of Non-Steady Filtration of Fluids and Gases. Nedra, Moscow (1972)
11. Kochina, I.N., Mikhailov, N.N., Filinov, M.V.: Groundwater mound damping. Int. J. Eng. Sci. **21**(4), 413–421 (1983)
12. Barenblatt, G.I.: Scaling, Self-similarity, and Intermediate Asymptotics. Cambridge University Press, Cambridge (1996)
13. Dussan, E.B. V, Auzerais, F.M.: Buoyancy-induced flow in porous media generated near a drilled oil well. Part 1. The accumulation of filtrate at a horizontal impermeable boundary. J. Fluid Mech. **254**, 283–311 (1993)
14. Huppert, H.E., Woods, A.W.: Gravity-driven flows in porous layers. J. Fluid Mech. **292**, 55–69 (1995)
15. Ennis-King, J., Paterson, L.: Engineering aspects of geological sequestration of carbon dioxide. In: SPE Asia Pacific Oil and Gas Conference and Exhibition, Melbourne, Australia, (77809-MS) (2002)
16. Nordbotten, J.M., Ceila, M.A., Bachu, S.: Injection and storage of CO_2 in deep saline aquifers: analytical solution for CO_2 plume evolution during injection. Transp. Porous Media **58**(3), 339–360 (2005)
17. Nordbotten, J.M., Celia, M.A.: Similarity solutions for fluid injection into confined aquifers. J. Fluid Mech. **561**, 307–327 (2006)
18. Hesse, M.A., Tchelepi, H.A., Orr, F.M.: Scaling analysis of the migration of CO_2 in saline aquifers. In: SPE Annual Technical Conference and Exhibition, San Antonio (SPE 102796) (2006)
19. Hesse, M.A., Tchelepi, H.A., Cantwell, B.J., Orr, F.M.: Gravity currents in horizontal porous layers: transition from early to late self-similarity. J. Fluid Mech. **577**, 363–383 (2007)
20. Hesse, M.A., Orr, F.M. Jr., Tchelepi, H.A.: Gravity currents with residual trapping. J. Fluid Mech. **611**, 35–60 (2008)
21. Juanes, R., MacMinn, C.W.: Upscaling of capillary trapping under gravity override: application to CO_2 sequestration in aquifers. In: SPE/DOE Symposium on Improved Oil Recovery, Tulsa (SPE 113496) (2008)
22. Juanes, R., MacMinn, C.W., Szulczewski, M.L.: The footprint of the CO_2 plume during carbon dioxide storage in saline aquifers: storage efficiency for capillary trapping at the basin scale. Transp. Porous Media (2009). doi:10.1007/s11242-009-9420-3
23. Bear, J.: Dynamics of Fluids in Porous Media. Courier Dover, Ballarat (1988)
24. Yortsos, Y.C.: A theoretical analysis of vertical flow equilibrium. Transp. Porous Media **18**(2), 107–129 (1995)
25. MacMinn, C.W.: Analytical modeling of CO_2 migration in saline aquifers for geological CO_2 storage. Master's thesis, Massachusetts Institute of Technology, Cambridge (2008). http://juanesgroup.mit.edu/cmac